AD-A228 100

REPORT DOCUMENTATION PAGE

Form Approved
OMB No. 0704-0188

1. AGENCY USE ONLY (Leave Blank)	2. REPORT DATE	3. REPORT TYPE AND DATES COVERED
	11 Jan 88	Conference Presentation

4. TITLE AND SUBTITLE
Application of Forced Unsteady Aerodynamics to a Forward Swept Wing X-29 Model

5. FUNDING NUMBERS
TA 2307-F1-38

6. AUTHOR(S)
J. Ashworth, T. Mouch, M. Luttges

7. PERFORMING ORGANIZATION NAME(S) AND ADDRESS(ES)
F.J. Seiler Research Laboratory
USAF Academy CO 80840-6528

8. PERFORMING ORGANIZATION REPORT NUMBER
FJSRL-PR-90-0010

9. SPONSORING/MONITORING AGENCY NAME(S) AND ADDRESS(ES)

10. SPONSORING/MONITORING AGENCY REPORT NUMBER

11. SUPPLEMENTARY NOTES

12a. DISTRIBUTION/AVAILABILITY STATEMENT
Distribution Unlimited

12b. DISTRIBUTION CODE

13. ABSTRACT (Maximum 200 words)

Numerous studies have hinted at possible use of controlled unsteady separated flows for lift enhancement on maneuvering aircraft. To verify these hypotheses and demonstrate application potential, an experimental study of forced unsteady flow fields about a 1/10 scale, reflection-plane model of the X-29 aircraft was conducted. Orthogonal view flow visualization was conducted with model angle of attack between zero and ten degrees and the canard angle of attack with respect to the model centerline between plus and minus 40 degrees. Static tests exhibit canard and wing stall characteristics and the upwash and downwash flow patterns. The dynamic (oscillating canard) tests demonstrate reduction of canard stall tendencies and decreased effective angles of attack at the wing root. Also, three-dimensional dynamic interactions were observed between the canard-generated leading edge vortices and the unsteady canard tip vortices. These complex flows convect downstream and impinge upon the wing. The interactions appear reproducible and controllable. Keywords:

14. SUBJECT TERMS
flow visualization; Sweptforward wings; Angle of attack; canard configurations; Wind tunnel models; vortices; Dynamic tests. (EDC)

15. NUMBER OF PAGES
13

16. PRICE CODE

17. SECURITY CLASSIFICATION OF REPORT	18. SECURITY CLASSIFICATION OF THIS PAGE	19 SECURITY CLASSIFICATION OF ABSTRACT	20 LIMITATION OF ABSTRACT
UNCLASSIFIED	UNCLASSIFIED	UNCLASSIFIED	NONE

AIAA'88

AIAA-88-0563
Application of Forced Unsteady Aerodynamics to a Forward Swept Wing X-29 Model

J. Ashworth, T. Mouch, and M. Luttges, HQ USAFA/DFAN, U.S. Air Force Academy, Colorado Springs, CO

AIAA 26th Aerospace Sciences Meeting
January 11-14, 1988/Reno, Nevada

APPLICATION OF FORCED UNSTEADY AERODYNAMICS TO A FORWARD SWEPT WING X-29 MODEL

J. Ashworth*, T. Mouch** and M. Luttges***
HQ USAFA/DFAN
U. S. Air Force Academy
Colorado Springs, Colorado 80840-5701

ABSTRACT

Numerous experimental and theoretical studies over the past few years have yielded results which hint at the possible aerodynamic benefits of utilizing controlled unsteady separated flows for lift enhancement on maneuvering aircraft. To verify these proposed hypotheses and demonstrate application potential, an experimental study of forced unsteady flow fields about a 1/10 scale, reflection-plane model of the X-29 aircraft was conducted. During these experiments, orthogonal view flow visualization data were collected with variation of the model angle of attack between 0° and 10° and the canard angle of attack with respect to the model centerline between ±40°. To qualitatively define the effects of dynamic sinusoidal oscillation of the canard, the model was first tested under static (nonoscillating canard) conditions. These static tests exhibit canard and tandem wing stall characteristics. Particularly well illustrated were the upwash and downwash flow patterns about this complex geometry model. The dynamic (oscillating canard) tests demonstrate aerodynamically beneficial reduction of canard stall tendencies and decreased effective angles of attack of the root area of the forward swept wing. Also, three-dimensional dynamic interactions were observed between the canard-generated leading edge vortices and the unsteady canard tip vortex patterns. These complex flows convect downstream and impinge upon the tandem forward swept wing. Though complex, the observed interactions appear reproducible and controllable characteristics that increase the likelihood of eventual application.

*Major, USAF
Associate Professor, Department of Aeronautics, U. S. Air Force Academy, Colorado Springs, Co.
Member AIAA

**Captain, USAF
Instructor, Department of Aeronautics, U. S. Air Force Academy, Colorado Springs, Co.
Member AIAA

***Professor, Department of Aerospace Engineering Sciences, University of Colorado, Boulder, Co.
Member AIAA

NOMENCLATURE

AOA	Model angle of attack
c	Canard chordlength measured at midspan
K	Nondimensional reduced frequency parameter, $K = \omega c/2V_\infty$
V_∞	Freestream tunnel velocity
α	Canard angle of attack relative to the model centerline
α_m	Mean angle of attack (degrees)
α_ω	Oscillation amplitude (degrees)
ϕ	Nondimensional oscillation phase angle (% of the cycle beginning at α_{max})
ω	Rotational frequency in radians per second

INTRODUCTION

Extensive experimental investigations on two-dimensional airfoils[1-9] and three-dimensional straight and swept wings[10-19] indicate possible aerodynamic advantages of forced unsteady flows. These dynamic flow fields may be utilized by high performance aircraft to expand flight envelopes in the low airspeed regime. In this regime of low airspeed and high AOA, aircraft maneuvering capability[20] depends on the control surface lift and stall characteristics. Due to the enhanced steady flow maneuvering qualities of the forward swept wing/canard configuration, it appears to be an exemplary combination[21-28] for initial studies on the feasibility of applying unsteady flow technology to advanced aircraft.

Initial investigations on a one-tenth scale, reflection-plane model of the X-29 aircraft were conducted to provide insight into the flow interactions likely to be produced by such aircraft configurations in an unsteady separated flow environment. Flow visualization techniques were utilized for these initial tests to provide qualitative definition of the complex unsteady flow fields about the

model. These visualized flows also allow prediction of critical flow areas where quantitative flow measurements must be obtained to fully define the unsteady flow phenomena. All tests were designed to give insight into the feasibility of using unsteady flows to enhance aircraft aerodynamics and to evaluate the flight mechanics needs of bringing such technology to fruition.

Low speed aircraft handling characteristics may be enhanced by the careful control of unsteady flows. In canard-configured aircraft, for example, flight qualities at low speeds and high angles of attack are dependent on flow separation characteristics about both the canard and wing. The subsonic flow about either of these tandem surfaces affects the overall flow patterns within which the aircraft must perform. Unsteady oscillation of the canard may enhance lift and delay flow separation from the canard upper surface. The downwash produced by the canard may also reduce the effective angle of attack of the trailing wing. Since the forward swept wing stalls from root-to-tip, this canard-induced effective angle reduction may delay root stall and provide for higher aircraft angle of attack operation. To examine these and other possible effects, flow visualization comparisons between both static and dynamic configurations of the X-29 were accomplished for various AOA's and reduced frequency parameter values.

METHODS

The 1/10 scale reflection-plane model of the X-29 aircraft was tested in the 60.9cm by 60.9cm test section, low turbulence wind tunnel at the University of Colorado. Throughout the X-29 model tests, the tunnel velocity was maintained at 25 feet per second. One side wall with splitter plate supported the model while the opposite wall was fitted with glass to permit flow visualizations. The top and bottom walls as well as the model and splitter plate were painted black to reduce reflections and enhance flow structure clarity.

The visualization smoke was introduced into the flow using two different techniques; a smoke rake located in the plenum chamber and a smoke wire positioned from top to bottom of the test section upstream of the model. The smoke rake technique provided a vertical plane of streamwise smoke lines through the test section spaced approximately one inch apart. The model was positioned in the tunnel so the plane of smoke impinged the canard at the midspan location. Under certain test conditions, the streaklines at critical locations were not as visible as desired due to the spatial gap between the lines. Therefore, a smoke wire technique[13] was used for increased flow clarity throughout the flow field about the canard and wing. The smoke wire could also be positioned to introduce the vertical smoke sheet at any desired span location across the canard or wing.

The X-29 reflection-plane model is mounted to a splitter plate which extends from top to bottom of the test section. The model can be rotated about a point near the center of gravity to change the angle of attack (AOA) of the entire model. A small D.C. motor and scotch yoke are mounted outside the tunnel and are affixed to the canard attachment shaft. This assembly induces sinusoidal canard pitching motions of variable frequency and amplitude. Flow visualization photography using stroboscopic illumination with both a 35mm camera and a high speed 16mm movie camera recorded the flow patterns. Photographic procedures were adjusted to capture the pertinent three-dimensional flow patterns about both the canard and the wing. To record the flow data, photographs were taken from many angular perspectives ranging from side to rear views.

The X-29 investigations began with static experiments. During these static tests, the model AOA was set at 0°, 5° and 10° while the canard α was varied in 5° increments between 0° and 40°. This canard α was always measured with respect to the model centerline. The data recording was accomplished using only the smoke rake technique. This procedure provided smoke visualization which first impinged the model at the midchord of the canard. Both side and rear view photographs were taken with the 35mm camera.

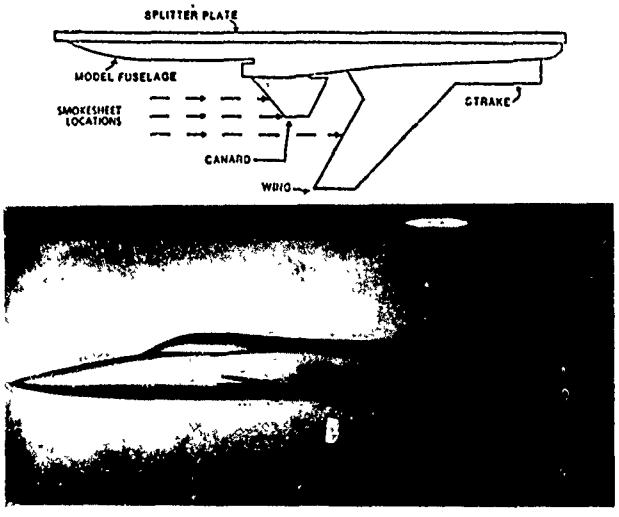

Fig. 1 Planform top view and side view photo of 1/10-scale model of the X-29 aircrart.

The dynamic tests also included model AOA values of 0°, 5° and 10° as well as parameter variations in the canard α_m of 0°, 5° and 10° and α_q of ±5°, ±10° and ±20°. The data collection methods included using both the smoke rake and

smoke wire techniques with the 35mm camera and the 16mm high speed camera. During the smoke wire tests, the wire was adjusted to position the smoke sheet to impinge on the canard leading edge at three locations: (1) at the canard midspan, (2) at the canard tip, and (3) to pass outboard of the canard tip by 6.5cm (Fig 1). The cameras were positioned to record side and rear view visualizations as well as an intermediate angular point between these two perspectives.

RESULTS

Visualization techniques applied to the X-29 model show the complex geometric structure of this aircraft configuration. The model geometry is shown in a planform diagram and side view wind tunnel photo in Fig 1. The large interactive flow area produced between the canard and the trailing wing shows intricate vortical structures. These are somewhat difficult to capture visually and the detailed vortical flow development is sometimes sacrificed to enhance the clarity of general flow characteristics about the tandem surfaces.

Both the canard and wing planforms elicit complex three-dimensional flow patterns. The canard planform is tapered and consists of an aft swept leading edge and a forward swept trailing edge. Although finite wing flow characteristics were observed about the canard, this tapered configuration and small thickness ratio prevent exact comparisons with previous oscillating wing experiments. The wing leading edge planform also contains both forward and aft swept profiles. The predominant forward swept span intercepts the aft swept region near the root location where the smoke impinges the surface. This aft-swept/forward-swept planform has been observed[24] to produce inboard and then outboard spanwise flows which converge and create a leading edge crank disturbance. This effect is quite predominant at high model angles of attack. Exact flow characteristics attributed to the crank are not investigated.

Static Tests

To facilitate unsteady flow comparisons, the model was first tested under static AOA and α conditions. Flow visualization techniques can only illustrate possible aerodynamic benefits of forced unsteady flows when static and dynamic comparisons are accomplished at similar test conditions. However, since the possible flight advantages of unsteady flows appear to be both the reduction of cataclysmic canard stall and the delay of forward swept wing root stall, the static test parameters were chosen to establish geometric conditions where such adverse effects were likely to be produced. Three model angles of attack of 0°, 5°, and 10° were tested each with nine canard angles of 0° to 40°. Data were recorded using side and rear view photographic perspectives.

When the model centerline is aligned with the freestream velocity (0° AOA), the steady flow characteristics at low canard α values are very smooth and attached about both the canard and wing. The potential flow region away from the control surfaces shows little disturbance due to the flow about the canard and wing. At α = 10° a separation bubble begins to form near the leading edge of the canard. The smoke streamlines show a decreased effective angle of attack (approximately 3° to 4°) on the wing due to the downwash from the canard. As α increases to 15°, the separation region over the canard increases in size, but the overall flow remains attached and the downwash angle increases another 2° to 3°. Presumably, the adverse pressure gradient finally causes complete flow separation observed over the canard at α = 20°. This separation is accompanied by an apparent increase in effective angle of attack of the wing. The smooth, cohesive flow lines over the top of the wing appear attached to the surface and exhibit little apparent turbulence for canard angles of 0° to 20°. As canard angle increases through 25° and up to 40°, the wake behind the canard increases in size and this turbulent, random streakline region is observed to pass over both top and bottom surfaces of the wing.

At 5° AOA, the wing is at a higher angle of attack and circulation has apparently increased. This increase is demonstrated by flow line differences about both the wing and canard. At small canard α values (0° to 10°), flow lines passing under the canard are observed moving upward and over the top surface of the wing. The very low pressure region created on the lifting wing upper surface produces an upwash effect in front of the wing leading edge. This wing upwash is also seen as an effective angle of attack increase on the canard. As the canard α increases to 10°, a separation region completely engulfs the top surface of the canard. Further increases in the canard α cause total flow separation and the separated wake completely engulfs the wing. At canard angles above 25°, the smoke lines flow around the canard tip. No apparent tip vortex forms suggestive of an absence of any effective pressure difference from one to the other side of the canard. This increasing α sequence is shown for the side view in the right column of Fig 2.

The complex, three-dimensional flow patterns about the model at 5° AOA are shown from both side and rear views in Fig 2. Spanwise flow characteristics which produce the distinctive patterns observed in previous side view visualizations can

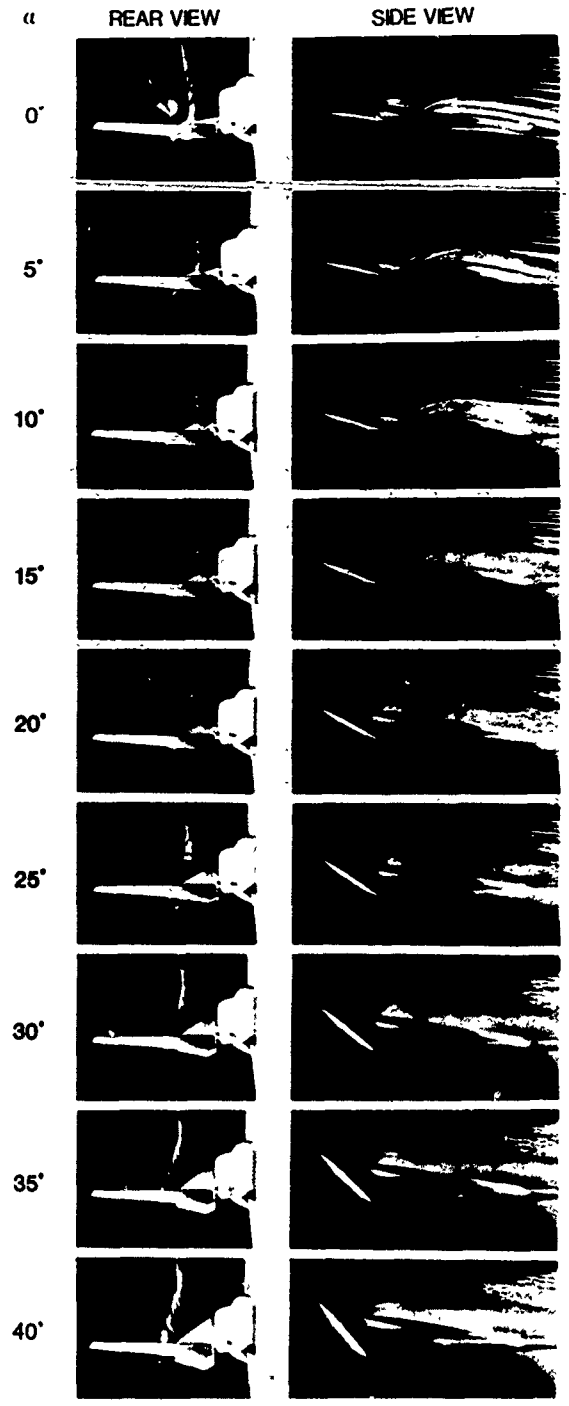

Fig. 2 Static rear and side view photos, AOA = 5°, α = 0° to 40°.

be seen in the rear view photos for canard angles of 0° to 40°. The horizontal smoke lines which pass with the freestream flow from left to right in the side view photographs are seen as vertically stacked lines flowing toward the camera in the rear view visualizations. At $\alpha = 0°$, the two overlapping side view patterns are caused by spanwise flow differences over top and bottom surfaces of the canard. The smoke lines intercept the canard at midspan. The lower surface flow is drawn outboard by the tip vortex. The smoke is captured into the tip vortex and traces a rotational flow well above the top surface of the wing. Thus, an outboard to inboard rotational pattern is viewed over the wing top surface. The smoke lines passing over the top of the canard remain nearly two-dimensional as they pass over the surface of the canard and wing. At $\alpha = 5°$, a separation bubble begins to form on the canard top surface and the tip vortex appears more turbulent in side view and less distinct in rear view photos. Lower streaklines, not engulfed by the tip vortex, are pulled outboard under the canard and then move upward against the wing lower surface as they traverse under the wing. Similar flow structures exist at $\alpha = 10°$ with a more turbulent tip vortex (shown by a diffused smoke pattern). As α increases to 15°, the canard stall is complete and the tip vortex is nearly indiscernible. Flow passing under the canard is still drawn up toward the wing lower surface. From $\alpha = 20°$ to 40°, the separation is exaggerated and flow lines can be traced around the canard surface in the rear view photos. The smoke lines are observed to loop outward around the canard and are drawn back toward the wing surface before the distinct smoke patterns dissipate into turbulence.

When the model AOA is increased to 10°, the flow separation over the canard initiates even at $\alpha = 0°$. At this AOA, an increased effective angle of attack of the canard is produced by wing upwash. The flow over the wing top surface is more turbulent than in the lower AOA cases. Flow passing under the canard is again drawn upward over the upper surface of the wing. Similar to the AOA of 5° test, two distinct flow patterns appear over the top surface of the wing. One passes under the canard near the tip and protrudes well above the flow pattern near the upper wing surface. A second, seemingly more inboard flow, passes over the top of the canard and then follows the contour of the upper surface of the wing.

These static investigations illustrate numerous three-dimensional flow characteristics observed from multiple exposure photographs. Such three-dimensionality appears both as changes in smoke line direction and cohesion. Increasing model AOA increased apparent circulation of the wing up to AOA = 10° where the flow shows weak separation tendencies near the root. This increase in AOA also created upwash (approximately 5°) which increased the effective canard angle of attack. Increasing the canard angle of attack from 0° to 40° established canard stall onset angles for each tested AOA of the model. Also, increasing canard α increased the canard downwash and decreased effective angle of attack of the wing until canard stall occurred. Before canard stall was complete, the canard tip vortex intensity increased with increasing canard α. These observations established

desired parameter ranges and reference flow conditions for the dynamic investigations.

Dynamic Tests

The unsteady flow fields produced by sinusoidally oscillating the canard of the X-29 model not only influence the immediately adjacent canard flow but also the dynamic characteristics occurring about the trailing wing. The static model experiments demonstrate flow fluctuations as model AOA and canard α vary. These flow alterations are shown as changes in stall angles, upwash and downwash, effective angles of attack, canard tip vortex appearance, and turbulence levels. To thoroughly comprehend dynamic flow patterns, variations in these flow characteristics were examined throughout a complete oscillation cycle. Changes in these flow characteristics as well as in other unique flow phenomenon are noted as the dynamic pitching cycle varied from ϕ = 0.0 to 1.0. Where applicable, comparisons are made between static and dynamic results as well as between various dynamic configurations. Flow visualization techniques were employed at different model angles, canard mean angles, canard oscillation amplitudes and reduced frequencies to attempt possible prediction of dynamically beneficial patterns.

Initial experiments were concerned with small amplitude oscillations that might be applicable to the computer controlled canard angular deflections of the X-29 aircraft. Dynamic flow visualizations of small amplitude (±5°) oscillations at constant nondimensional reduced frequency, K = 1.0, were initially examined. Since static tests show that model AOA changes the static stall angle of the canard, the mean angle of attack for oscillation was varied for each AOA during dynamic tests in order to project the canard above and below the static stall. As AOA increased by 5° for each test, the mean angle about which oscillations occurred was decreased by 5°. Thus, the canard oscillation angles remained constant with respect to the freestream flow.

Initial investigations on the model were conducted at model AOA of 0° and mean angle of 10°. At maximum canard angle of attack, ϕ = 0.0, the flow lines are attached to both the canard and wing. This same angle of attack when used during static tests produced a separation bubble which engulfed the entire upper surface of the canard. At ϕ = 0.1 (one tenth of the way through the pitching cycle), a leading edge vortex is discernible on the upper surface of the canard. The canard wake appears more turbulent and downwash from the canard reduces the effective angle of attack of the wing root, possibly to negative values. As ϕ increases through 0.2 and 0.3, the leading edge vortex increases in size and the turbulence in the canard wake under the wing surface increases. The downwash from the canard and attached flow over the wing are verified by the bending of those smoke streaklines well above and remote to each surface. These streaklines bend upward reflecting disturbances in the mean flow created by the two control surfaces and bend downward between the two surfaces when the greatest downwash is observed. This bending of the streaklines located well above the X-29 surfaces also was seen to be correlated with downwash during the static tests.

Near ϕ = 0.5, the leading edge vortex dissipates on the canard surface much like the three-dimensional vortex dissipation observed during other finite wing experiments. From ϕ = 0.6 to 0.9, the canard is pitching upward toward maximum angle of attack. The leading edge vortex has dissipated into a viscous shear layer. The canard downwash decreases during this portion of the cycle and is evidenced by the straighter, more horizontal smoke lines seen well above the canard and wing surfaces. Although the downwash fluctuated during the pitching cycle, the flow remained attached to the canard surface throughout with disturbances only during the presence of the highly cohesive leading edge vortex structure. Similar to static tests at this AOA, smoke from the midspan region was not drawn outboard to mark the canard tip vortex.

For model AOA values of 5° and 10° and mean angles of 5° and 0°, the wing increased circulation is verified by the upwash affecting the smoke flow over the canard and wing surfaces. Much like static tests at these AOA values, the canard tip vortex flow is marked by smoke from the midspan region and is pulled up over the top surface of the wing. This indicates three-dimensional effects on the canard which cause the lower surface smoke flow to be trapped by the tip vortex and trace this swirling pattern about the wing surface. The leading edge vortex formation on the top surface of the canard occurs earlier in the pitching cycle for the higher AOA values. This earlier formation is accompanied by larger vortical structures which begin to show minimal convection tendencies across the canard surface. However, the leading edge vortex is not observed to influence the trailing wing flow. Similar to the static tests, the higher AOA investigations show the canard tip flow passing well over the top surface of the wing throughout the pitching cycle. Also, the canard downwash does not appear as dominate as in the lower AOA test.

When the oscillation amplitude was increased from ±5° to ±10°, the spatial magnitudes of the ensuing unsteady phenomena increased. At this α_ω, a change

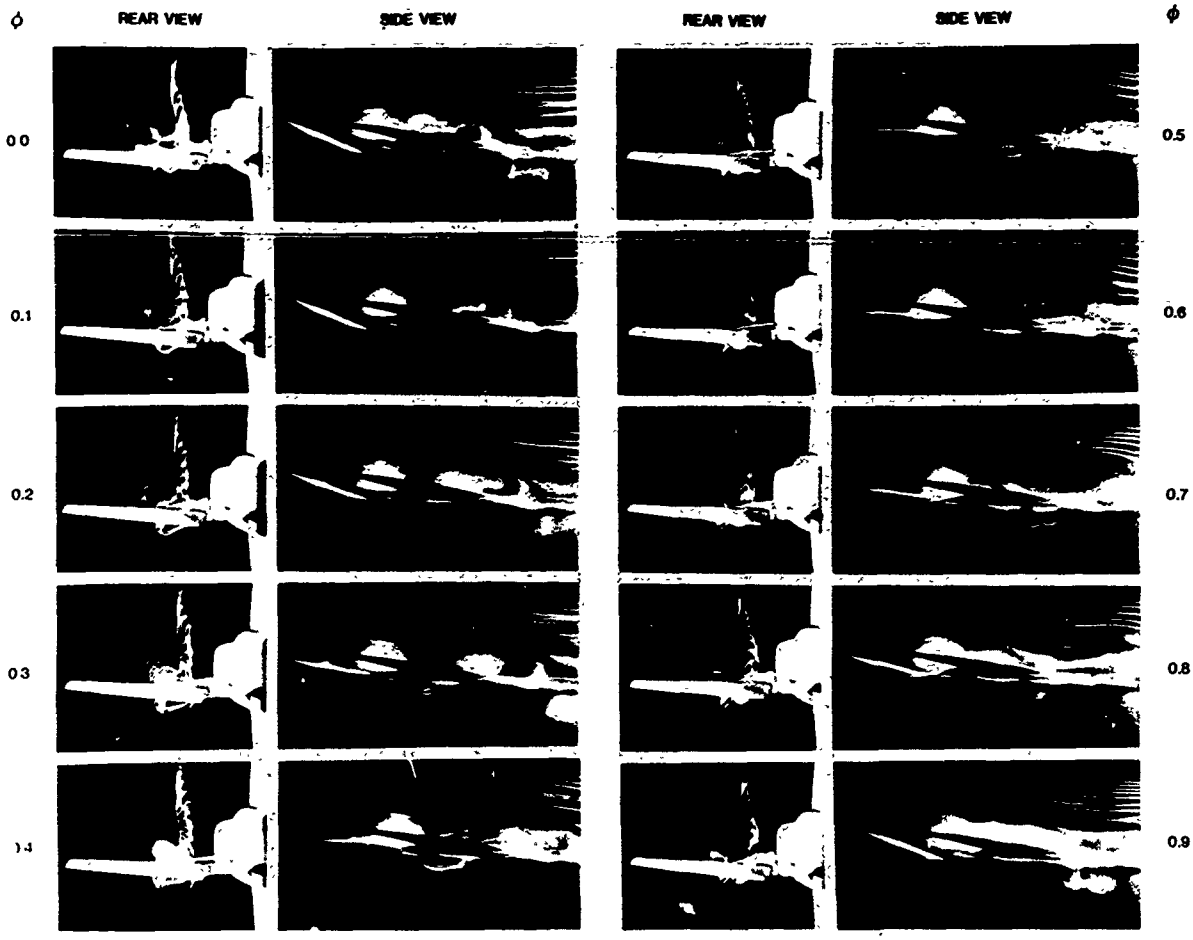

Fig. 3 Dynamic rear and side view photos, K = 1.0, AOA = 5°, α_m = 5°, α_ω = ±10°, ϕ = 0.0 to 0.9.

in the model AOA stimulated flow characteristic changes similar to those observed at lower α_ω values but with increased magnitudes. Generally, for this α_ω, the canard leading edge vortices were larger in size and demonstrated more rapid convection and shedding tendencies than were observed during the lower amplitude tests. Since the angular range of motion of the canard was increased, the cyclic downwash and upwash produced by the canard causes greater downward and upward flows about the wing surface. The maximum angle of attack phase of the canard pitching cycle creates a downward protrusion of smoke to beneath the wing surface. Likewise, the minimum α phase causes the shed canard flow to pass above the wing top surface. Shedding of the leading edge vortex from the canard surface temporally coincides with the low α phase of the pitching cycle. Due to this coincidence of shedding of the leading edge vortices and the upwash from the canard wake, it is difficult to access the exact contribution of either to the flow about the trailing wing. A series of side and rear view photographs for one complete oscillation cycle are shown in Fig 3.

To facilitate analysis of the three-dimensional effects, rear view photographs were taken for model AOA of 5°, mean angle of 5° and oscillation amplitude of ±10°. The rear and side views at identical dynamic conditions are shown in Fig 3. The rear view photographs do not contain the entire flow pattern over the surfaces due to lighting and camera focal length restrictions. Since the area of significant flow description is just forward and aft of the canard trailing edge, this horizontal surface is used for camera focus. The smoke flow patterns proximal to the canard trailing edge will appear most prominent in the photographs.

At ϕ = 0.0, the smoke lines passing about the canard and wing surfaces demonstrate the complex three-dimensionality of this flow. Similar to static rear view data, the smoke is pulled out of the original vertical plane by dynamic spanwise pressure gradients. The smoke flow over the canard appears reasonably two-dimensional as it convects across the canard and wing surfaces. The smoke flow under the canard is pulled from left to right toward the canard tip. This smoke is entrained in the canard tip vortex and traces the swirling pattern

upward and well above the wing upper surface. The rear view visualization shows this vortex pattern as a vertical line extending upward from the canard tip with a circular smoke pattern above the wing. For ϕ = 0.1 and 0.2, the rear view flow patterns are similar to those observed at ϕ = 0.0. The flow under the canard is drawn farther away from the lower surface as left-to-right flow toward the tip continues. A canard tip vortex is still observed with the vortex center moving closer to the surface of the wing as increases. A slightly three-dimensional leading edge vortex can be seen from the rear as a vertical disturbance on the canard surface. As ϕ increases through 0.3 to 0.6, the rear view canard tip vortex moves even closer to the wing surface. A decrease in apparent strength is indicated by a decreasing smoke diameter around the vortex center. The left-to-right spanwise smoke flow under the canard moves farther away and then closer to the canard lower surface. This characteristic, accounting for flow temporal delay for traversing velocity, is signaled by the flow moving around the canard surface at the high α portion of the pitching cycle then moving closer during low α. Another smoke trace is also now observed under the wing surface in vertical line with the original smoke flow. This trace originates above the canard and indicates the spanwise location of the lower surface protrusion. At ϕ = 0.6, this trace near the wing root position becomes very clear. The corresponding side view shows a distinct rotating vortex under the wing at this position. The remaining cycle, ϕ = 0.7 to 0.9, illustrates an increase in canard tip vortex influence and a dissipation of the under-wing vortex core.

The effects of reducing K value from 1.0 to 0.5 were examined. In these tests, the model AOA and mean angle of attack were both set at 5° and the oscillation amplitude was ±5°, ±10° and ±20°. An initial analysis of the data reveals four overall trends. First, the smoke lines passing near any control surface are more turbulent than for the higher K value cases. There also appears to be little if any canard tip vortex flow up over the top surface of the wing. The leading edge vortices formed on the canard surface cyclically grow in size then dissipate, with no apparent effect on the flow over the top surface of the wing. And finally, all the unsteady flow patterns seem directly related only to the cyclic upwash and downwash created by the canard oscillating motion.

To facilitate the qualitative definition of spanwise variations in the complex flow about the model, a smoke wire technique was employed to position the smoke sheet at various spanwise locations on the canard. Fig 4 shows photographs of the flow impinging on the canard leading edge at midspan, canard tip and a location

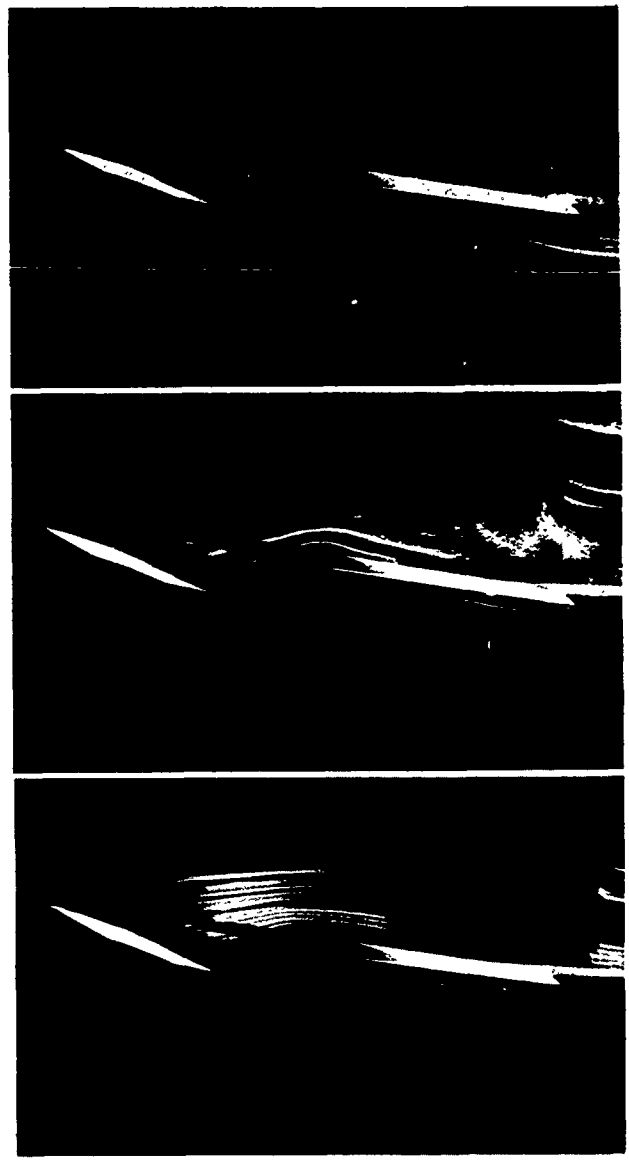

Fig. 4 Spanwise comparisons, K = 1.0, AOA = 5°, α_m = 5°, α_ω = ±10°, smoke introduced
Top: canard midspan,
Middle: canard tip,
Bottom: 6.5cm outboard.

outboard of the canard tip. The temporal phase position of all three photographs is ϕ = 0.1. The outboard position shows little effect of the canard as the flow passes the canard and flows about the surface of the wing. The canard midspan and tip locations illustrate the canard leading edge and tip vortex interactions as well as the canard wake flow about the wing.

A well-defined leading edge vortex is seen on the canard upper surface at the midspan location. The high circumferential velocity of this vortex draws the potential flow down across the aft portion of the surface thus preventing any flow separation at this moderate angle of attack. The canard wake flow impinging on the wing is multidirectional. The flow

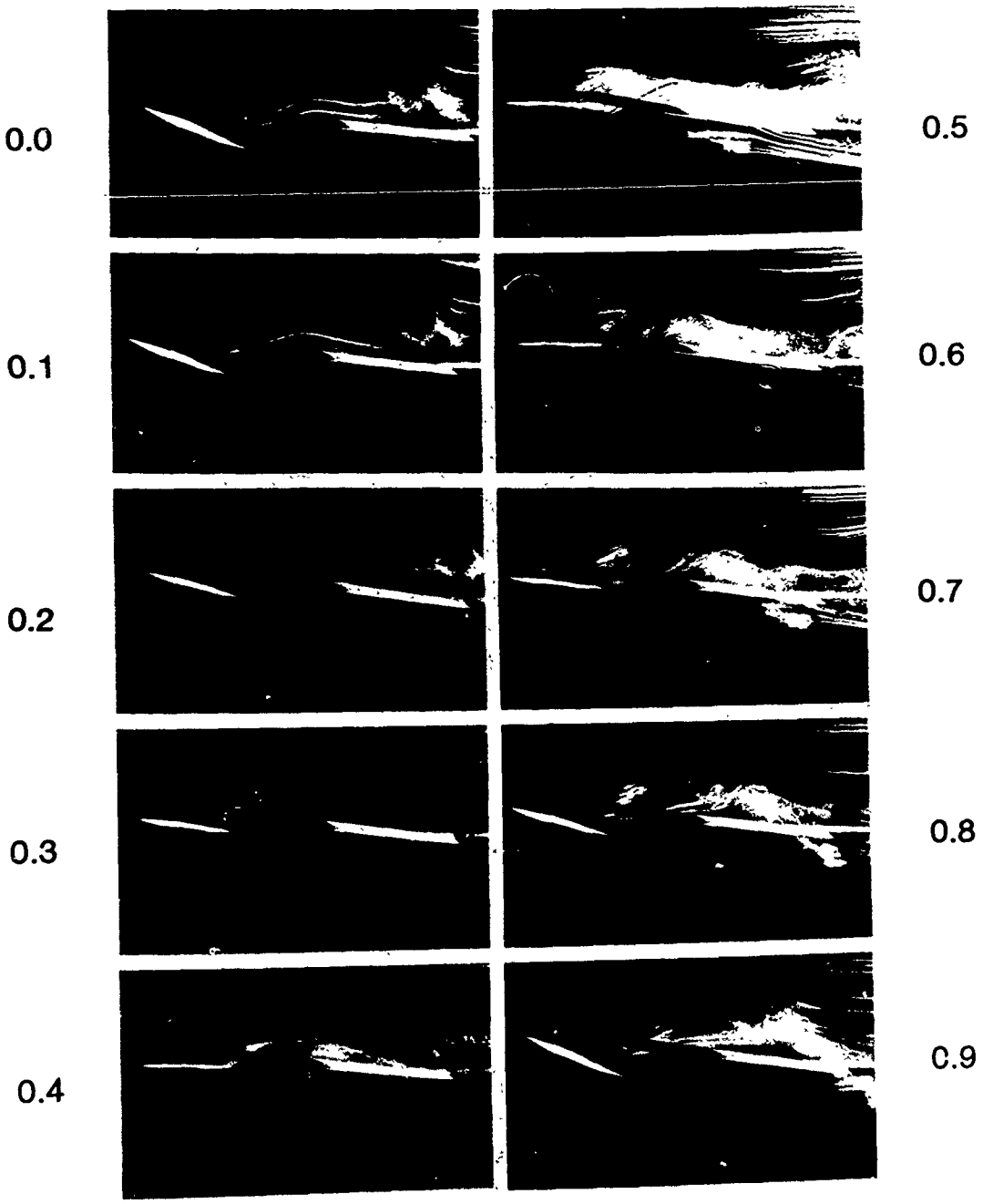

Fig. 5 Dynamic side view photos, K = 1.0, AOA = 5°, α_m = 5°, α_ω = ±10°, ϕ = 0.0 to 0.9, smoke introduced at canard tip.

passing over the circumference of the vortex is shown as downwash passing under the wing while the flow passing under the canard is pulled outboard and is shown as an upwash in front of the wing surface.

Smoke flow impinging on the canard at the tip shows a somewhat different flow pattern. The streaklines pass around the canard tip and are entrained in the tip vortex. This three-dimensional vortex causes upward flow on the outboard portion and a downward flow on the inboard portion of the vortex. Streaklines passing near the leading edge of the canard are drawn inboard into the tip vortex and pass under the wing. However, the streaklines that pass near the trailing edge of the canard remain with the upward flow of the outboard portion of the tip vortex and pass above the wing surface.

To enhance comprehension of the complex flow interactions about the canard

and wing, a series of photographs depicting a complete oscillation cycle is shown in Fig 5. In this series, the smoke impinges on the canard at the tip. When the-canard is at high angles of attack (ϕ = 0.0 and 0.1), a tip vortex is observed on the canard with streamwise rotational characteristics as described above. As the canard α decreases through ϕ values of 0.2 and 0.3, the tip vortex about the canard appears to decrease in strength. The more cohesive portion of this streamwise vortex traverses with the flow and is divided by the leading edge of the wing. Part of the tip vortex passes over the wing while the lower portion passes under the wing. This splitting of the tip vortex is traced above and below the wing throughout the remainder of the cycle. At ϕ = 0.4, the strength of the tip vortex decreases further and the smoke is drawn inboard to mark the position of the leading edge vortex as it approaches the trailing edge of the canard. At ϕ = 0.5 The leading edge vortex is observed shedding from the trailing edge of the canard slightly upstream of the upward portion of the tip vortex. Throughout the remainder of the cycle and into the early stages of the next cycle, the leading edge vortex is observed traversing across the upper surface of the wing in tandem with the flow disturbance from the upper portion of the canard tip vortex. Different perspective photographs and high speed photography show the canard leading edge vortex core and the core of the canard tip vortex to be connected and continuous. This overall angle-shaped vortex (similar to half a horseshoe vortex) is shed cyclically from the surface of the canard and impinges on the surface of the wing.

DISCUSSION

The complex geometry of the X-29 model precipitates unique three-dimensional airflow patterns during both static and dynamic tests. Flow visualization techniques were used to record these patterns and demonstrate flow characteristics. The multiple-exposure, stroboscopic photography utilized during both static and dynamic tests verified flow field reproducibility and illustrated turbulence domains. Smooth, cohesive smoke line contours indicated completely superimposed streaklines and consistent flow patterns throughout the multiple exposure photos. The random, multi-streaklined appearances signify the more turbulent flows. Some highly turbulent regions appear as faint, white areas due to the smoke diffusion and light illumination.

The bending of cohesive streaklines in front of, behind and well above the canard and wing surfaces depicts flow alterations caused by parameter changes. Angular deflections of the smoke lines in front of the canard, when compared with model centerline, indicate upwash and effective angle of attack increase of the canard. The flow lines passing near the surface of the canard and then about the wing surface show canard downwash and the resulting effective angles of attack on the wing. This pattern of upwash and downwash also can be seen in the bending of flow lines far above the surfaces.

Variations in canard angle of attack during static tests caused upwash, downwash, wingtip and turbulence level changes in the overall flow field. As α increased, the canard downwash increased and wing effective angle of attack decreased until complete canard stall occurred. This fully developed stall also eliminated the tip vortex and created a large turbulent wake region behind the canard. Of course, useful flight characteristics may be lost when the canard angle reaches that of full stall. The three-dimensional flow traces around the canard tip at very high angles of attack indicate a high drag, low lift condition. Yet, the wing root may still be generating lift at higher AOA values.

Variations in model AOA caused similar flow disturbances in both static and dynamic tests. Since the model centerline was varied in 5° increments, the wing geometric angle of attack also changed by this amount. An increase in model AOA caused upwash and effective angle of attack increase. In turn, the increases produced earlier static canard stall and larger dynamic canard leading edge vortices. A three-dimensional effect is seen at model AOA of 5°and 10° that was not observed when the model centerline was aligned with the freestream flow. At 5° and 10° AOA, the smoke flow under the canard is pulled outboard and entrained in the canard tip vortex. This marked tip vortex is observed for most high AOA test conditions and it generally passes well above the wing top surface.

In the small amplitude (±5°) oscillation tests, model AOA and mean angle of attack changes kept the angular oscillations constant with respect to the tunnel freestream. As model AOA increased, the mean angle was decreased. Therefore, the observed effects resulted principally from the flow field changes due to the model and wing angle of attack. The canard leading edge vortices were larger in size and initiated only slightly earlier for the higher model AOA test conditions. Canard leading edge vortex formation and convection tendencies were identical at each AOA for this oscillation amplitude. Identical unsteady flow characteristics were observed for higher amplitude (±10°) oscillations with increased angular travel producing flow alterations of slightly larger magnitude.

The sinusoidal pitching motion of the canard produced cyclic effective angle of attack changes on the wing. Such

effective α cycles were shared by upper and lower wing surface protrusions. When the canard begins the increasing angle of attack phase of the cycle, the downwash from the canard begins to increase and this decreases the effective angle of attack of the wing. This downwash, traced by the path of the smoke flow, extends well beneath the lower surface of the wing. When the canard sinusoidally reverses angular sign and begins the decreasing α portion of the cycle, the downwash decreases and the wing effective angle of attack increases. Exact flow description of this area can only be achieved using measured flow properties such as pressure and velocity.

The streamwise vortex shed from the canard tip is split by the wing leading edge and part of this rotating structure passes both above and below the wing surface. The cyclic disturbance passing over the top surface of the wing appears to be caused by a combined effect of traversing leading edge vortex and upward rotational flow from the split tip vortex. The canard tip vortex is split by the wing leading edge at the cycle phase where the leading edge vortex is shed from the canard trailing edge. Therefore, the upstream edge of the shed canard tip vortex contains the leading edge vortex shed from the canard. The cores of the two vortices are observed to be connected with the result that the tandem shedding forms into a single angular (half horseshoe shaped) vortex. Such vortex integration has been postulated in earlier studies on aft swept three-dimensional wings[14].

Reducing K value had the effect of increasing turbulence levels and decreasing any traversing tendencies of the canard leading edge vortex. The turbulence levels of the flow aft of the canard increased for all oscillation amplitudes tested. Flow patterns in front of the canard seemed nearly unchanged by the lowered K values. The canard leading edge vortex cyclically developed then dissipated into a shear layer with little evidence of convection or shedding. The canard tip vortex was not marked by the smoke drawn outboard along the lower canard surface. These characteristics suggest a possible reduction in pressure intensities during the lower K value tests.

CONCLUSIONS

The very complex geometry of the X-29 model makes analysis of variations caused by a single parameter change difficult. Static and dynamic flow visualization photography serves to minimize comparative flow analysis difficulties and to maximize the identification of flow characteristics which may encompass beneficial unsteady flight conditions. The present technique is limited to comparative analyses. A complete flow field investigation must include both velocity and pressure measurements. The visualized flow patterns seen here, when analyzed using known physical flow properties such as stall, upwash, downwash and tip effects, can be extrapolated to the identification of phenomena that may possess aerodynamic utility.

Slow airspeed, high angle of attack flight of the static model substantiates the existence of adverse flow conditions where some type of aerodynamic flow control device may be beneficial. Increased model AOA caused early canard stall and, possibly, disruptive wing lifting conditions in the wake of the stalled canard. Higher AOA values also seemingly created exorbitant three-dimensional effects as shown by increased spanwise flow on the canard and overlapping flow patterns about the wing. The advantages of applied unsteady flow producing devices may well be found in the maintenance of attached flow at high AOA values over both the canard and wing surfaces.

Dynamic sinusoidal oscillations of the canard produce cyclic unsteady flow fields about the canard and wing which may be beneficial in delaying separation. Airflow in the immediate vicinity of the canard remains attached to the canard surface throughout the pitching cycle. The major disturbance of the airflow is founded in the formation and development of the leading edge vortex. This dynamic vortex formation has been shown in numerous airfoil and wing tests to be beneficial in enhancing lift characteristics. Therefore, the increased overall flow attachment and the cohesive leading edge vortex development on the surface of the canard may increase lift production well above static, high angle of attack values.

Increased flow attachment on the canard surface causes a nearly continuous downwash aft of the canard. This decreases the effective angle of attack of the wing in the root area. The stall characteristics of the forward swept wing have been shown to be from root-to-tip. Therefore, this decrease in effective angle of attack near the root area may delay the overall onset of separation on the wing. Further investigations at multiple span locations across the wing span reveal the exact spanwise separation tendencies and should pinpoint the contribution of the unsteady flow arising from the canard.

The disturbances on the surface of the wing are caused mainly by the cyclic shedding of canard vortices and the upwash-downwash changes. Such complex flow patterns cannot be fully characterized with flow visualization data alone. These areas of complex flows acting on lifting surfaces must be

examined using other flow measuring techniques such as hot wire anemometry and surface pressure. Under dynamic conditions, the shedding canard vortices exhibit cyclic three-dimensional structures which may produce very complex flow field variations across the wing surface. Although the flow fields reported here are produced by oscillating motion, similar unsteady structures may be formed when the X-29 aircraft rapidly changes canard angle of attack.

ACKNOWLEDGMENTS

This work is supported, in part, by the U.S. Air Force Office of Scientific Research, Grant F4962083K0009, Dr. James McMichael, project manager. The technical assistance of W. Bank and R. Meinzer is appreciated.

REFERENCES

1. McCroskey, W.J., Carr, L.W. and McAlister, K.W., "Dynamic Stall Experiments on Oscillating Airfoils," AIAA-75-125, AIAA 13th Aerospace Sciences Meeting, Pasadena, California, Jan. 1975.

2. McCroskey, W.J., "Unsteady Airfoils," Annual Review of Fluid Mechanics, 1982, pp. 285-311.

3. McAlister, K.W. and Carr, L.W., "Water Tunnel Visualizations of Dynamic Stall," Journal of Fluids Engineering, Vol. 1D1, Sept. 1979, pp. 376-380.

4. Luttges, M.W., Robinson, M.C. and Kennedy, D.A., "Control of Unsteady Separated Flow Structures on Airfoils," AIAA-85-0531, AIAA Shear Flow Control Conference, Boulder, Colorado, March 1985.

5. Robinson, M.C. and Luttges, M.W., "Unsteady Flow Separation and Attachment Induced by Pitching Airfoils," AIAA-83-0131, AIAA 21st Aerospace Sciences Meeting, Reno, Nevada, Jan. 1983.

6. Robinson, M.C. and Luttges, M.W., "Unsteady Separated Flow: Forced and Common Vorticity About Oscillating Airfoils," Workshop on Unsteady Separated Flows, Francis, M. and Luttges, M. (eds.), University of Colorado: 1984, pp. 117-126.

7. Helin, H.E., Robinson, M.C. and Luttges, M.W., "Visualization of Dynamic Stall Controlled by Large Amplitude Pitching Motions," AIAA-86-2281-CP, AIAA Atmospheric Flight Mechanics Conference, Williamsburg, Virginia, Aug. 1986.

8. Reisenthel, P.H., Nagib, H.M. and Koga, D.J., "Control of Separated Flows Using Forced Unsteadiness," AIAA-85-0556, AIAA Shear Flow Control Conference, Boulder, Colorado, March 1985.

9. Reynolds, W.C. and Carr, L.W., "Review of Unsteady, Driven, Separated Flows," AIAA Shear Flow Control Conference, Boulder, Colorado, March 1985.

10. Adler, J.N., Robinson, M.C., Luttges, M.W. and Kennedy, D.A., "Visualizing Unsteady Seperated Flows," Third International Symposium on Flow Visualization, Proceedings, Vol. III, Ann Arbor, Michigan, Sept. 1983, pp. 806-811.

11. Adler, J.N. and Luttges, M.W.,"Three-Dimensionality In Unsteady Flow About a Wing," AIAA-85-0132, AIAA 23rd Aerospace Sciences Meeting, Reno, Nevada, Jan. 1985.

12. Ashworth, J. and Luttges, M.,"Comparisons in Three-Dimensionality in the Unsteady Flows Elicited by Straight and Swept Wings," AIAA-86-2280CP, AIAA Atmospheric Flight Mechanics Conference, Williamsburg, Virginia, August 1986.

13. Ashworth, J., Waltrip, M. and Luttges, M.,"Three-Dimensional Unsteady Flow Fields Elicited by a Pitching Forward Swept Wing," AIAA-86-1104, AIAA 4th Joint Fluid Mechanics, Plasma Dynamics and Lasers Conference, Atlanta, Georgia, May 1986.

14. Ashworth, J., Huyer, S. and Luttges, M.,"Comparisons of Unsteady Flow Fields about Straight and Swept Wings Using Flow Visualization and Hotwire Anemometry," AIAA-87-1334, AIAA 19th Fluid Dynamics, Plasma Dynamics and Lasers Conference, Honolulu, Hawaii, June 1987.

15. Freymuth, P., Finaish, F. and Bank, W., "Visualization of Wing Tip Vortices in Accelerating and Steady Flow," Journal of Aircraft, Vol. 23, No. 9, Sept. 1986, pp. 730-733.

16. Freymuth, P., "The Vortex Patterns of Dynamic Separation: A Parametric and Comparative Study," Progress in Aerospace Sciences, Vol. 22, 1985, pp. 161-288.

17. Gad-el-Hak, M. and Ho, C., "Three-Dimensional Effects on a Pitching Lifting Surface," AIAA-85-0041, AIAA 23rd Aerospace Sciences Meeting, Reno, Nevada, Jan. 1985.

18. Gad-el-Hak, M. and Ho, C.," Unsteady Vortical Flow Around Three-Dimensional Lifting Surfaces," AIAA Journal, Vol. 24, No. 5, pp. 713-721, May 1986.

19. Carta, F.O.," Unsteady Stall Penetration of an Oscillating Swept Wing," Workshop on Unsteady Separated Flows, Francis, M. and Luttges, M. (eds.), University of Colorado: 1984, pp. 28-37.

20. Herbst, W.B., "Supermaneuverability," Workshop on Unsteady Separated Flows, Francis, M. and Luttges, M. (eds.), University of Colorado: 1984, pp. 1-9.

21. Landfield, J.P. and Rajkovic D., "Canard/Tail Comparison for an Advanced Variable-Sweep-Wing Fighter," Journal of Aircraft, Vol. 23, No. 6, June 1986.

22. Robinson, M.C., Helin, H.E. and Luttges, M.W., "Control of Wake Structure Behind an Oscillating Airfoil," AIAA-86-2282-CP, AIAA Atmospheric Flight Mechanics Conference, Williamsburg, Virginia, Aug. 1986.

23. Uhuad, G.D., Weeks, J.M. and Large, R., "Wind Tunnel Investigation of Transonic Aerodynamics Characteristics of Forward Swept Wings," Journal of Aircraft, 20(3), March 1983, pp. 195-202.

24. Griffin, K.E., Haerter, E.C. and Smith, B.R., "Wake Characteristics and Interactions of the Canard/Wing Lifting Surface Configuration of the X-29 Forward-Swept Wing Flight Demonstrator," USAFA-TN-83-7, 15 Aug. 1983.

25. Moore, M. and Frei, D., "X-29 and Forward Swept Wing Aerodynamic Overviews," AIAA-83-1834, AIAA Applied Aerodynamics Conference, Danvers, Massachusetts, July 1983.

26. Whipple, R.D. and Ricket, J.L., "Low-Speed Aerodynamic Characteristics of a 1/8-Scale X-29A Airplane Model at High Angles of Attack and Sideslip, " NASA Technical Memorandum 87722, Sept. 1986.

27. Tierney, J., "The Real Stuff," Science 85, American Association for the Advancement of Science, Sept. 1985.

28. Hoey, B., "Experimental: As in X-29A," AIRMAN, Vol. XXIX, No. 4, AFRP 30-15, pp. 28-34, April 1985.